TURBULENT PIPE FLOW DOWNSTREAM A 90° BEND: CURVATURE RATIO EFFECTS

A. Kalpakli Vester[1], *R. Örlü*[1] *and P. H. Alfredsson*[1]

[1] *KTH CCGEx and Linné Flow Centre, KTH Mechanics, 100 44 Stockholm, Sweden*

ramis@mech.kth.se

1 Introduction

Turbulent flows in curved pipes are encountered widely in technical applications such as in gas pipelines, nuclear reactors, heat exchangers, internal combustion engines etc. While such flows have been studied extensively with respect to global quantities (such as pressure drop, heat transfer) due to their direct practical relevance (*Vashisth et al. 2008*) the fluid physics of such flows have not been investigated within the fluid dynamics community as much as their counterparts in straight pipes.

When a fluid passes through a curved pipe, the particles located near the axis of the pipe are moved away from the centre of the pipe towards the outer pipe wall. The cause for this is the counteraction of an adverse pressure gradient with the centrifugal forces arising from the curvature. The first analytical solution for a laminar flow in an infinitely long curved pipe was given in *Dean 1928* where it was shown that in such a geometry two counter-rotating vortices exist; a flow pattern known today as Dean vortices.

Laminar flow in curved pipes is well understood and has been studied thoroughly through the years due to its relevance to biological and physiological mechanisms (*Chandran and Yearwood 1981, Glenn et al. 2012*).

On the other hand, the physical mechanisms of turbulent flow through curved pipes are not fully understood. Even though a number of studies on such flows exist they mainly provide integral quantities and single-point statistics through single-point measurement techniques (*Enayet et al. 1982, Sudo et al. 1998*). Quantitative visualisations—in order to obtain information on the behaviour and dynamics of both the primary and secondary flow field in time—are important and require whole-field measurement techniques. It is well known that in laminar flow, the Dean vortices are symmetrical with respect to the geometric plane of symmetry. Although, this is the case for turbulent flows on average, it has been shown that in 90° bends, the vortices appear to oscillate in time (*Brücker 1995, Sakakibara and Machida 2012*). This mechanism has been know in the literature as "swirl-switching". The first to observe the divergence of the Dean vortices from the classical twin vortex pattern in the case of turbulent flows in sharp bends were *Tunstall and Harvey 1968*. The cause for this was believed to be separation at the inner bend. However, after almost four decades, it was shown through large-eddy simulations (LES) in a sharp and mild bend (the latter for which separation does not occur) that the swirl-switching exists regardless of the appearance of separation at the inner bend corner (*Rütten et al. 2005*). More recently, the phenomenon was investigated (again in a sharp bend) by means of proper orthogonal decomposition (POD) and it was thought to be caused by a single mode depicting a single cell spanning the whole pipe cross-section (*Hellström et al. 2013*). In general, most studies dealing with the swirl-switching phenomenon, are experimental and provide data for sharp bends (*Brücker 1995, Sakakibara and Machida 2012, Hellström et al. 2013*), whereas there is only one study (*Rütten et al. 2005*) providing LES data for two different bends, a sharp and mild one, considering the effect of curvature and separation on the oscillatory character of the Dean cells.

The present investigation provides the first experimental data for two different bends (a mild and a sharp one) aiming to fill this gap in literature *i.e.* explore the effect of the acuteness of the bend on the swirl-switching phenomenon. Moreover, the evolution of the time-averaged flow field with downstream distance from the bend is documented.

2 Experimental set up & technique

The experiments were conducted in the CICERO laboratory at KTH where a compressor installation facility is capable of delivering air at a maximum mass flow rate of 500 g/s at 6 bar. In order to ensure steady flow conditions, the mass flow rate is monitored by a hot-film type mass flow meter (ABB Thermal mass flow meter FMT500-IG), that is mounted 10 m upstream the rotating valve.

Experiments were conducted downstream a sharp bend and a mild bend, mounted at the exit of a $80D$ long straight pipe. The bends are of circular cross section and have an inner diameter of $D = 40.5$ mm. The sharp bend used for the measurements has a centreline radius of $R_c = 51$ mm and the mild one has $R_c = 144.5$ mm, yielding curvature ratios of $\gamma = R/R_c = 0.17$ and 0.39, respectively. Data from cross-sectional

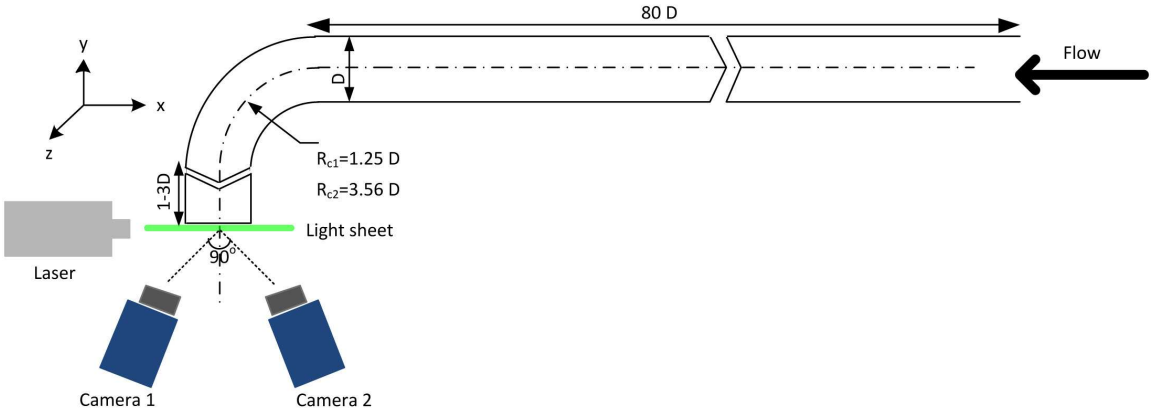

Figure 1: Schematic of the experimental setup as well as the TS-PIV system (*top view*). $D = 40.5$ mm, $R_c = 51$ mm for the sharp bend and $R_c = 144.5$ mm for the mildly curved pipe used in the experiments. The laser light sheet is aligned at the immediate vicinity of the pipe bend exit.

fields were acquired at $1D$, $2D$ and $3D$ downstream distances from the bend exit both for the sharply and mildly curved pipe. The nominal Reynolds number for all cases, based on the pipe diameter and the bulk velocity W_b is $Re = W_b D/\nu = 2.3 \times 10^4$, where ν is the kinematic viscosity. The flow parameters were chosen to be close to the ones used in the LES by *Rütten et al. 2005* and it is expected that in the mildly curved pipe separation will not occur at the inner bend. However it should be kept in mind, that in the present study, the existence of separation at the inner bend corner was not investigated.

Time-resolved stereoscopic particle image velocimetry (TS-PIV) was used to obtain two-dimensional, three-component (2D-3C) cross-sectional flow fields downstream the pipe bend. To seed the flow, standard olive oil was atomised using a high volume liquid seeding generator (10F03 Seeding Generator, DANTEC Dynamics). The resulting smoke was injected continuously through four holes drilled symmetrically around a steel pipe section mounted far enough upstream of the bend in order to avoid effects on the flow from the smoke injection. A laser light sheet of approximately 1 mm thickness was produced by a Nd-YLF laser (Pegasus, 10 kHz maximum frequency, New Wave Research).

Two high-speed C-MOS cameras (Fastcam APX RS, Photron, 3000 fps at full resolution 1024×1024 pixels, 10 bit) were positioned at an angle of approximately 90° between their viewing axes in backward-forward scatter. Two Nikon Nikkor lenses with focal length of 105 mm, were adjusted using a Scheimpflug adapter. For the in-situ calibration of the cameras, images were taken of a home made calibration target positioned alternatively in two planes, in the plane of the light sheet and in a plane 0.5 mm in the downstream direction. The traversing of the calibration target was done by means of an accurately machined ring with the same diameter as the pipes and a spacing of 0.5 mm.

The number of image pairs per recording was 3000 and they were taken with a sampling frequency of 1 kHz. However, for one case at $z/D = 2$ with the sharp bend mounted, the recording was repeated successively five times, providing in total 15000 snapshots in order to assess statistical convergence. The post-processing of the data was performed with the commercial software DaVis 7.2, LaVision GmbH. The vector fields were calculated with a multi-pass iteration procedure for increased resolution starting with an interrogation window of 64×64 pixels and decreasing to 16×16 pixels with an overlapping area of 50%. Outliers were detected by a median test and replaced by a linear interpolation scheme.

Due to low frequency oscillations associated with the swirl-switching phenomenon and the necessity to secure a finely resolved spectra of the time series in order to obtain the frequency of those oscillations, long sampling times are needed. The PIV data sets were therefore compared with time series data obtained via laser-Doppler velocimetry (LDV). The LDV measurements were also performed at the exit of the two bends at $z/D = 2$ using a single component Dantec FlowLite system in conjunction with a BSA 60 processor (Dantec Dynamics). The emitting light source is a 10 mW He-Ne laser with wavelength of 632.8 nm. The liquid used to seed the flow for the LDV measurements was the same as for the PIV measurements. The sampling time was 50 sec and the sampling rate varied from around 18 kHz at the centreline down to around 6 kHz at the position closest to the wall.

3 Results

Time-averaged flow field

The development of the mean flow field at different stations downstream the two curved pipes with curvature ratios $\gamma = 0.39$ and 0.17 will be presented in the

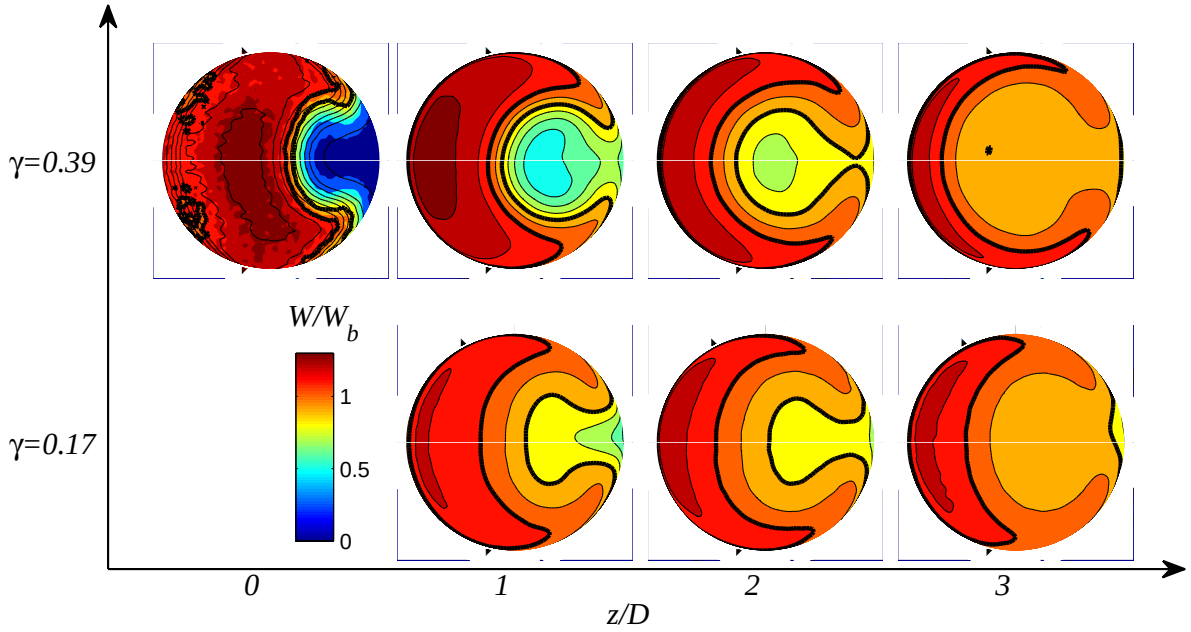

Figure 2: Contours of the mean streamwise (W) velocity component scaled by the bulk speed (W_b) for 0.2, 1, 2 and 3 diameters (D) downstream distance from the bend exit and for two curvature ratios: $\gamma = 0.17$ and 0.39. The contours corresponding to velocities 0.9 and $1.1W_b$ are shown with thicker black lines. For the $z/D = 0.2$ case the flow field was smoothed using a 20×20 px box filter. The inner wall is to the right whereas the outer wall is to the left of the subplots. The region close to the wall has been blinded out due to spurious vectors.

following. The statistics shown here were computed over 3000 PIV realisations acquired during 3 sec. This yields about 750 integral time scales which was found to provide converged mean statistics.

Figure 2 shows contour maps of the time-averaged streamwise velocity component scaled by its bulk value (obtained from integration of the streamwise velocity field) for three downstream stations ($z/D = 1$, 2, 3) and for two curvature ratios. For comparative purposes, available data for $\gamma = 0.39$ and $z/D = 0.2$ which were obtained in a previous setup (*Kalpakli et al. 2013*) are also included. However, the different parameters for this case compared to the present setup should be kept in mind, as for example the shorter development length of the flow until it reaches the curved pipe section. Furthermore, due to the short distance from the bend exit in that case and thus the large velocity gradient, a spatial filter was necessary to be applied in order to achieve comparable degree of focus on the large scale structures as in the other cases.

It is observed that in all cases, the high velocity fluid is pushed towards the outer wall whereas the slower moving fluid is deflected towards the inner wall creating a C-shaped velocity distribution. The mean maximum velocity reaches $1.3W_b$. The milder the curvature of the bend, the smaller the centrifugal forces, therefore the smaller the velocity gradient created along the pipe cross-section. As can be anticipated, the flow relaxes progressively and the curvature effects appear to be damped considerably even at the $3D$ station, however the distance from the bend is too small to consider flow recovery. The development of the Dean cells as well as the magnitude of the in-plane velocities as function of the curvature ratio and the downstream location is shown in Fig. 3. There is a clear decrease in the strength of the secondary motion for the mildly curved bend. The maximum velocity value of $0.5W_b$ for the sharp bend decreases to $0.15W_b$ for the mild bend, whereas the counter rotating cells tend to move towards the inner wall in the latter case. A clear decrease in the magnitude of the in-plane velocities is observed also as the flow develops downstream the bend for both the mild and sharp bend.

Time-resolved flow fields

In order to illuminate the effect of curvature on the swirl-switching and its constituting modes, POD is employed on the TS-PIV data and the results from this analysis are presented in this section. Results from LDV measurements will also be included in order to support the conclusions drawn from the TS-PIV measurements. Here, results only for one downstream station at $z/D = 2$ are shown.

The three most energetic POD modes (excluding the mode representing the mean) are shown in Fig. 4 as sectional streamlines for the mild bend. The first mode appears as a single cell spanning the whole cross-section with its centre located close to the inner pipe wall. The direction of rotation of that modes is of opposite signs with downstream location (not shown here) with a clockwise rotation at $z/D = 1$ and an

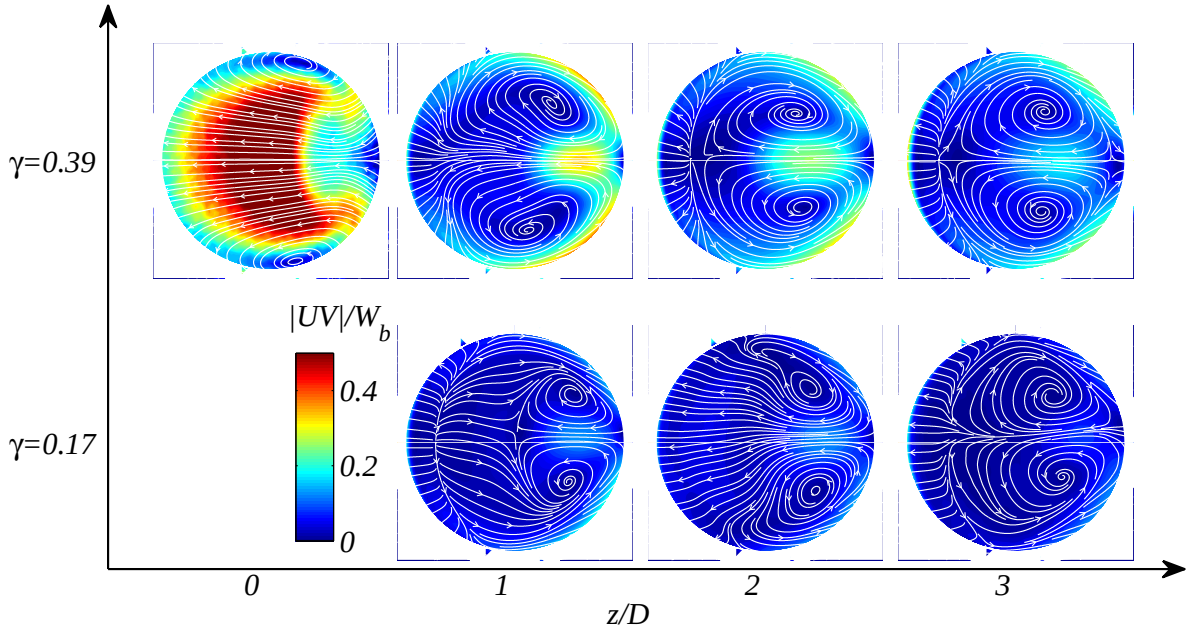

Figure 3: Contours of the magnitude of the in-plane velocity components ($|U_{xy}|= \sqrt{(U^2+V^2)}$) scaled by the bulk speed and sectional streamlines (white) of the time-averaged secondary flow field. The maximum value of the velocity magnitude (red) corresponds to $0.5W_b$. The streamlines have been smoothed using a moving average with $t = 0.02$ sec. Same configuration as in Fig. 2.

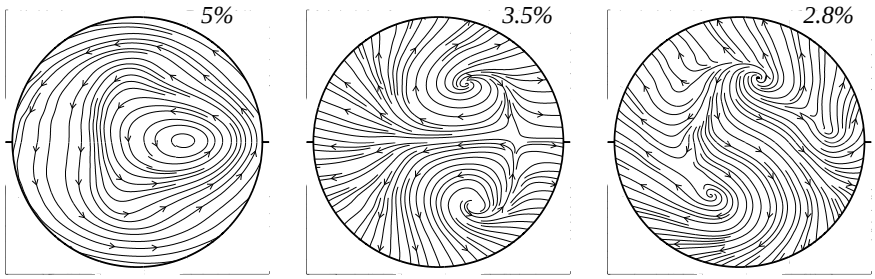

Figure 4: The first three POD modes plotted as sectional streamlines for $\gamma = 0.17$ and $z/D = 2$. The percentage amount of energy content relative to the sum of the energy of all modes (excluding the mean) is given for each mode.

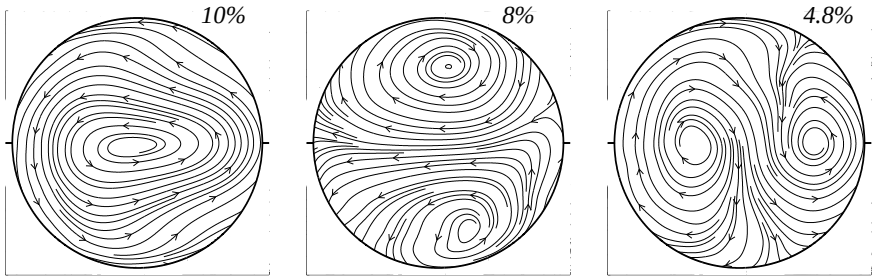

Figure 5: The first three POD modes plotted as sectional streamlines for $\gamma = 0.39$ and $z/D = 2$. The percentage amount of energy content relative to the sum of the energy of all modes (excluding the mean) is given for each mode.

anti-clockwise one at $z/D = 2$. Modes 2 and 3 show cells that appear less well-shaped than the well-known Dean vortices.

Considering the first three POD modes for the sharp bend in Fig. 5, it is observed that a single cell mode, spanning the whole pipe cross-section, appears as the most energetic feature located almost at the centre of the pipe. The direction of its rotation changes in time in the anti-clockwise and clockwise sense (not shown here). For the two other modes, a Dean-like flow appears with one of the cells being suppressed. This modal pattern agrees well with the one shown

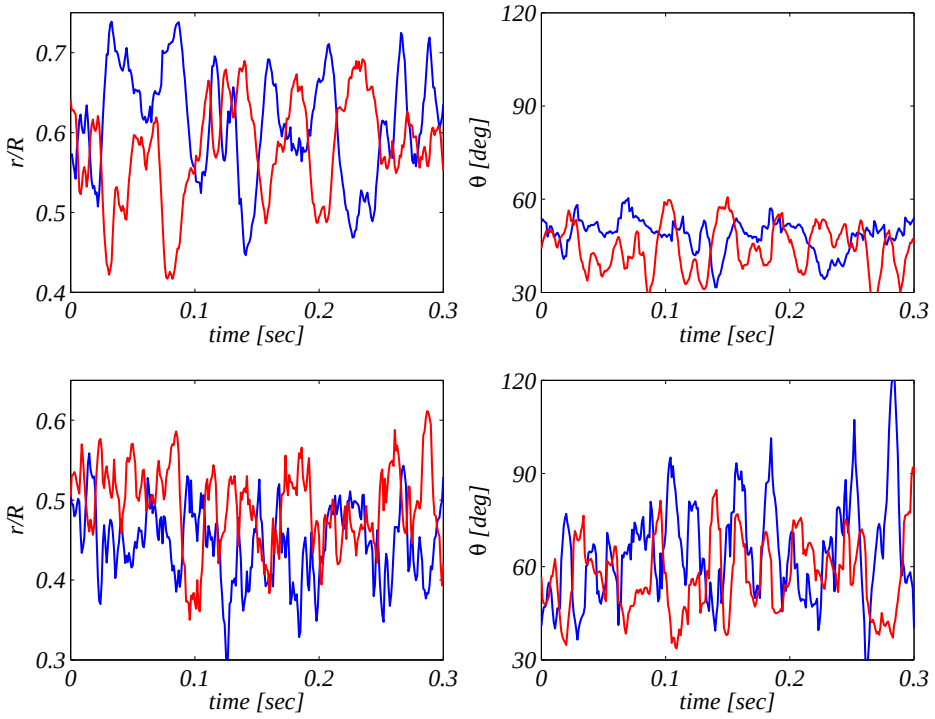

Figure 6: Time series of the distance (r) between the location of the upper (blue) and lower (red) vortex core and the centre of the pipe and their respective angles (θ) for $z/D = 2$. Here the time series have been smoothed using a moving average with $t = 0.01$ sec. *Left:* $\gamma = 0.17$, *Right:* $\gamma = 0.39$. Note that here the absolute angle of the vortex core has been taken to enhance the correlation between the two vortices.

in *Hellström et al. 2013*, where a single cell was observed as the most energetic mode and was thought to be the cause of the swirl switching, whereas modes 2 and 3 showed tilted Dean cells with one the vortices being suppressed. However, the differences between the two studies *i.e.* curvature ratio, downstream location, sampling rate etc, should be kept in mind.

In an effort to examine where in the pipe cross-section the switching can be detected and whether it is a single- or double-mode phenomenon, complementary LDV measurements were performed at different heights on the pipe y-axis and across the horizontal axis. Well-converged probability density functions (PDF) of the vertical velocity could be obtained through the LDV measurements.

Figure 7 shows the PDF map of the vertical velocity component for different positions along the horizontal axis of the pipe and at $y/R = 0.04$ both for the mild and sharp bend at $z/D = 2$. It is clear, that for the sharp bend, the PDF exhibits a bi-modal behaviour close to the inner wall having two peaks at positions between $x/R = 0.6$ to 0.9. The double-peaked PDF at $x/R = 0.8$ is shown in an insert for clarity. The shape of the PDF shows that there indeed exists a quasi-periodic motion. This agrees well with the findings of *Brücker 1995* and *Kalpakli and Örlü 2013* where the spectra of the tangential velocity close to the inner wall showed two peaks at low frequencies, believed to be related to the swirl-switching mechanism. However, for the mild bend the PDF exhibits small "wiggles" but no clear bimodal behaviour can be observed. It is also noted that comparing the PDF maps between the two bends, even though the time-averaged velocity profiles do not differ considerably from each other, the PDFs span a larger margin for the case of the sharp bend.

In an effort to further study how the Dean cells evolve as function of curvature ratio, the cells were tracked in time and their core locations were identified based on the minimum vorticity in the reconstructed flow field using the first four POD modes (considering the mode representing the mean and the modes shown in Fig. 4 and 5). Two approaches were undertaken: in the first one the upper and lower Dean vortex core was tracked individually from each other by applying the algorithm on the upper ($0° < \theta < 180°$) or lower ($180° < \theta < 360°$) half of the pipe cross-section, respectively. In the second approach, the most dominant vortex was identified by applying the algorithm on the whole pipe cross-section. This was done in order to investigate which one of the two vortices is the dominating one at each time instance and if this "dominance" pattern exhibits a periodic behaviour.

Figure 6 shows the time series of the location of the upper and lower Dean vortex, tracked by considering only the upper or lower half of the pipe, respectively. The core angle is also shown both for the sharp and mild bend at $z/D = 2$. For both curvature ratios, it is clear that the time series exhibit a quasi-periodic char-

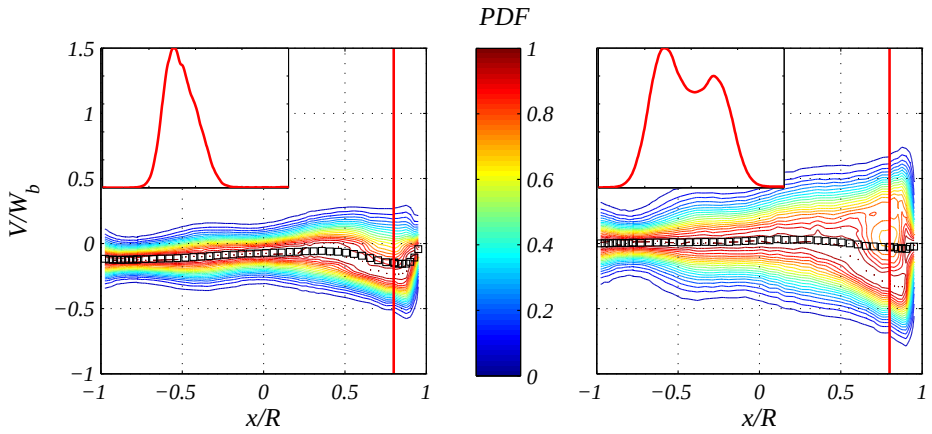

Figure 7: Probability density function (PDF) of the vertical velocity component (contour lines) scaled by the bulk speed and plotted together with its mean (black squares) along the horizontal pipe axis at $z/D = 2$ and $y/R = 0.04$. *Left:* $\gamma = 0.17$, *Right:* $\gamma = 0.39$. The insert depicts the PDF of the vertical velocity at $x/R = 0.8$ (red line). Data from LDV measurements.

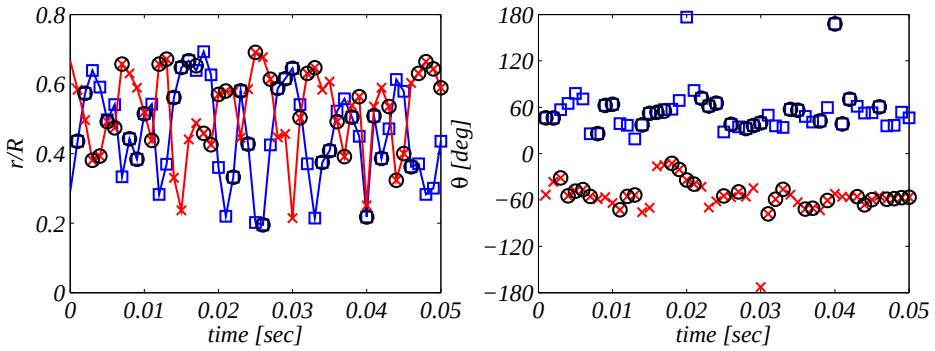

Figure 8: Time series of the distance (*left*) between the location of the upper (blue) and lower (red) vortex core and the centre of the pipe and their respective angles (*right*) for $z/D = 2$ and $\gamma = 0.39$. Black circles denote the most dominant vortex. Here, only a short time interval is shown to ease visualisation of the vortices' behaviour however for the conclusions a sampling time of 3 sec was considered.

acter whereas the two vortices are anti-correlated (a correlation coefficient of -0.6 and -0.5 was found for time series of the core radius for the mild and sharp bend, respectively). It is observed that for the sharp bend, the vortices move between a larger angle margin spanning from 40 to 120 degrees exhibiting a more oscillatory character than in the case with the mild bend.

In Fig. 8 the most dominant vortex from the upper or lower one, is identified by applying the tracking algorithm on the entire pipe cross-section. It is evident that the two vortices alternate in dominance but it is unclear if this is done in a periodic way. The total percentage number of the core locations found to coincide with the upper or lower vortex location is almost 97%, with the two vortices being equally dominant in time. This shows that it is indeed the two Dean vortices which are the dominant structures in the flow field and only in a few instances other significant vortices might appear.

4 Conclusions

Turbulent curved pipe flow is investigated as function of the curvature ratio, downstream location from the bend exit. Two curved pipes with $\gamma = 0.17$ and 0.39, denoting a mildly and sharply bended pipe respectively, have been used. The flow field has been quantitatively visualised by means of TS-PIV at three downstream locations from the bend, $z/D = 1$, 2 and 3. Mean fields, turbulence statistics, POD and vortex tracking have been used as data analysis tools.

It has been shown that the mean flow field changes significantly both in terms of the primary and secondary flow, with the change in curvature ratio and downstream position. As expected, the magnitude of the secondary flow is considerably damped when a mild bend is used. However, the vortical patterns between the sharp and mild bend as well as the downstream location from the bend, do not differ much. The main impact of increasing the curvature ratio is that the centre of the Dean vortices moves away from the inner wall and moves more towards the centre. Furthermore,

as the flow relaxes as the downstream distance from the bend exit increases, the Dean vortices for both the mild and sharp bend, tend to move towards the centre of the pipe.

POD showed the existence of a single cell occupying the entire cross-section as the most energetic mode for the sharp bend. This mode resembles closely the so-called "switching mode" which was assumed to cause the swirl-switching in *Hellström et al. 2013*. Furthermore, modes 2 and 3 showed the Dean vortices tilted with one of the cells being suppressed. For the mild bend, the modal pattern was slightly different; the tilted Dean vortices were not observed at $z/D = 2$. The PDF of the vertical velocity component from LDV measurements at $z/D = 2$, exhibits a bimodal behaviour close to the inner bend suggesting that the flow has a periodic character. For the sharp bend two distinctive peaks could be observed whereas for the mild bend those were identified as "wiggles" rather than clear peaks. By tracking the core of the Dean vortices for both bends and all stations, it was shown that the cores move in an anti-correlative and quasi-periodic manner as well as dominating equally in time the flow field. However, the vortices in the case of the sharp bend exhibited a more oscillatory character than the vortices in the mild bend. This indicates that the swirl-switching is affected by the acuteness of the bend curvature and it can possibly be correlated to the existence of separation at the inner bend.

Acknowledgments

This research was done within CCGEx, a centre supported by the Swedish Energy Agency, Swedish Vehicle Industry and KTH.

References

Brücker, C. (1995) A time-recording DPIV-study of the swirl switching effect in a 90° bend flow, Proc. 8th Int. Symp. Flow Vis., 1-4 Sept., Sorrento (NA), Italy.

Chandran, K. B. and Yearwood, T. L. (1981), Experimental study of physiological pulsatile flow in a curved tube, *J. Fluid Mech.*, Vol. 111, pp. 59–85.

Dean, W. R. (1928), The stream-line motion of fluid in a curved pipe, *Phil. Mag.*, Vol. 5, pp. 671–695.

Enayet, M. M., Gibson, M. M., Taylor, A. and Yianneskis, M. (1982), Laser-Doppler measurements of laminar and turbulent flow in a pipe bend, *Int. J. Heat Fluid Flow*, Vol. 3, pp. 213–219.

Glenn, A. L., Bulusu, K. V., Shu, F. and Plesniak, M. W. (2012), Secondary flow structures under stent-induced perturbations for cardiovascular flow in a curved artery model, *Int. J. Heat Fluid Flow*, Vol. 35, pp. 76–83.

Hellström, L. H. O., Zlatinov, M. B., Cao, G. and Smits, A. J. (2013), Turbulent pipe flow downstream of a bend, *J. Fluid Mech.*, Vol. 735, R7.

Kalpakli, A. and Örlü, R. (2013), Turbulent pipe flow downstream a 90° pipe bend with and without superimposed swirl, *Int. J. Heat Fluid Flow*, Vol. 41, 103–111.

Kalpakli, A., Örlü, R. and Alfredsson, P. H. (2013), Vortical patterns in turbulent flow downstream a 90° curved pipe at high Womersley numbers, *Int. J. Heat Fluid Flow*, Vol. 44, 692–699.

Rütten, F., Schröder, W. and Meinke, M. (2005), Large-eddy simulation of low frequency oscillations of the Dean vortices in turbulent pipe bend flows, *Phys. Fluids*, Vol. 17, p. 035107.

Sakakibara, J. and Machida, N. (2012), Measurement of turbulent flow upstream and downstream of a circular pipe bend, *Phys. Fluids*, Vol. 24, p.041702.

Sudo, K., Sumida, M. and Hibara, H. (1998), Experimental investigation on turbulent flow in a circular-sectioned 90-degree bend, *Exp. Fluids*, Vol. 25, pp. 42–49.

Tunstall, M. J. and Harvey, J. K. (1968), On the effect of a sharp bend in a fully developed turbulent pipe-flow, *J. Fluid Mech.*, Vol. 34, pp. 595–608.

Vashisth, S. Kumar, V. and Nigam K. D. P. (2008), A review on the potential applications of curved geometries in process industry, *Ind. Eng. Chem. Res.*, Vol. 47, pp. 3291–3337.